EXPERIMENTAL CELL RESEARCH **228,** 292–305 (1996)
ARTICLE NO. 0329

Apoptosis of L929 Cells by Etoposide: A Quantitative and Kinetic Approach

GABRIELLA BONELLI,*,[1] MARIA CRISTINA SACCHI,* GIUSEPPE BARBIERO,* FEDERICA DURANTI,* GIOVANNA GOGLIO,* LUDOVICA VERDUN DI CANTOGNO,* JOSEPH SALVATORE AMENTA,† MAURO PIACENTINI,‡ CARLO TACCHETTI,§ AND FRANCESCO MARIA BACCINO*,¶

**Dipartimento di Medicina ed Oncologia Sperimentale, Corso Raffaello 30, 10125 Turin, Italy; †Department of Pathology, University of Pittsburgh School of Medicine, Pittsburgh, Pennsylvania 15260; ‡Dipartimento di Biologia, Università di Roma Tor Vergata, 00173 Rome, Italy; §Istituto di Anatomia, Università di Genova, 16126 Genoa, Italy; and ¶Centro CNR di Immunogenetica ed Oncologia Sperimentale, 10126 Turin, Italy*

Exponentially growing L929 cells were continuously exposed to 1 or 10 μM etoposide (VP-16). The effects of such treatment on cell growth, cycle distribution, morphology, and selected biochemical events were examined. DNA synthesis rates were markedly decreased and the protein/DNA ratio increased (unbalanced growth). Growth was blocked, with most cells being cycle arrested by 24 h in (late S–)G2–M. An asynchronous process of cell death then developed. Cells initially shrank into eosinophilic, trypan blue-excluding bodies, which were then released into the medium, and eventually became permeable to trypan blue. Transmission electron microscopy confirmed that dying cells acquired an apoptotic morphotype, with compaction and margination of chromatin, loss of microvilli, and shrinkage of cytoplasm and nucleus. Tissue transglutaminase activity and intensity of immunostaining rapidly increased in treated cultures. Internucleosomal DNA fragmentation could not be detected by agarose gel electrophoresis, yet flow cytometry revealed that the apoptotic bodies had a very low DNA fluorescence ($\leqslant$10% of the 2n value). In agreement with the microscopic findings, this suggested that extensive DNA degradation had occurred in dead cells. While rates of cell loss from the monolayer amounted to 21 and 57% day^{-1} (1 and 10 μM VP-16, respectively), apoptotic indexes largely underestimated the extent of the process. These indexes only measured the accumulation of apoptotic bodies, i.e., the balance between their generation and disposal. The latter occurred by mechanisms similar to those that operate in tissues: "secondary necrosis" or phagocytosis by viable homotypic cells in the monolayer ("homophagy").

[1] To whom reprint requests should be addressed. Fax: 11-6707753; E-mail: bonelli@unito.it.

INTRODUCTION

The classical and most widely investigated models of apoptosis are based on cultures or fresh cell preparations in suspension. Such models usually employ cells of the hemopoietic lineages (thymocytes and many others), which almost always fully and promptly develop most features regarded as typical of the apoptotic process, such as the internucleosomal DNA fragmentation. Moreover, cells in suspension are more easily analyzed by techniques routinely used in studies on apoptosis, such as flow cytometry or transmission electron microscopy, with no need for the more demanding procedures required for monolayer cultures.

More recently, models based on monolayer tissue cultures have become increasingly frequent in the vast literature on apoptosis and have been dealt with adequately [e.g., 1–9], widening the spectrum of *in vitro* models of apoptosis that can be appropriately investigated by advanced cell biological techniques such as static cytofluorometry, electrophysiology, or imaging microscopy. Moreover, apoptosis in monolayer cultures not only involves dramatic changes in the general architecture of cells, but also detachment of the dying cells from the substrate into the medium, thus offering an easy opportunity to discriminate between viable and apoptotic cells [6, 8–9].

The present study illustrates the general properties of a model of apoptosis based on L929 cells grown in monolayer and continuously exposed over a 3-day period to etoposide (VP-16), an inhibitor of DNA topoisomerase II (topo II). Similar to another model system under study in our laboratories, namely, L cell monolayers exposed to excess thymidine [1, 2], apoptotic cell death by VP-16 develops as an asynchronous process that follows the blockade of the replicative cycle and begins not earlier than 24 h after treatment. Apoptosis was evaluated by morphology and flow cytometry, and cultures were examined for selected biochemical

0014-4827/96 $18.00

events. Moreover, cell loss was quantified kinetically from the decay of monolayer DNA radioactivity in prelabeled cultures. The present study shows that the kinetic approach is critical to fully appreciate the extent of a cell death process that, much as in most situations *in vivo*, occurred sparsely and asynchronously in the cell population. By contrast, the process was greatly underestimated by static parameters that measure, either microscopically or flow cytometrically, the frequency of apoptotic cells at selected time windows and thus only provide instant pictures.

MATERIALS AND METHODS

Cell culture and treatment. Monolayers of mouse L929 cells were grown in Dulbecco's modified minimal essential medium (DMEM) supplemented with 10% fetal calf serum, 100 U/ml penicillin, and 100 μg/ml streptomycin under standard conditions, in a water-saturated atmosphere of 5% CO_2 in air at 37°C. Cultures were routinely screened for mycoplasma infection by staining with the DNA-specific fluorochrome 4′,6-diamidine-2-phenylindoledihydrochloride (DAPI) and by an enzyme immunoassay (Boehringer Mannheim, Germany).

All experiments were started with unsynchronized exponentially growing cultures. Cells were seeded in petri dishes (Costar, U.S.A.) at a density of 15–20,000/cm^2 and 24 h later shifted (t_0) to medium with VP-16 added (from 34 m*M* stock solutions in DMSO) at concentrations ranging from 0.1 to 10 μM, as specified. The medium was changed daily to ensure a fairly constant drug concentration over the whole experimental period, the cultures being usually analyzed at 0, 24, 48, and 72 h of treatment.

Growth was measured both as cell number and as accumulation of protein or DNA in the monolayer. Cells harvested by trypsinization were counted in triplicate with an electronic particle counter (ZM; Coulter Electronics, Hialeah, FL). Protein and DNA were respectively determined by the method of Lowry *et al.* [10], with minor modifications, and the method of Boer [11] on cells detached mechanically with a rubber policeman and homogenized in PBS with a probe ultrasonic cell disruptor (MK2; MSE, UK).

Morphology. Monolayers grown on glass chamber slides (Nunc, U.S.A.) and treated with VP-16 as described above were carefully processed to minimize cell detachment, washed with PBS, fixed in 95% ethanol, air dried, and stained with hematoxylin and eosin. To better visualize chromatin, we fixed cultures as above and stained them in parallel with DAPI (10 ng/ml methanol). These cells were then washed with PBS followed by absolute ethanol, mounted in Bacto-FA (Difco, U.S.A.), and viewed in an epiilluminated fluorescence microscope (Dialux 20; Leitz, Germany).

For electron microscopy, cells ($4–6 \times 10^6$) harvested from the monolayer by trypsinization or from the medium by centrifugation were processed either separately or after pooling. After centrifugation, pellets were washed with PBS, fixed with 2.5% glutaraldehyde in 0.1 *M* cacodylate buffer, pH 7.3, postfixed with 1% (w/v) osmium tetroxide in the same buffer (15 min), stained with 1% (w/v) uranyl acetate in water (1 h), dehydrated in an ethanol ascending series, and embedded in LX112. Gray-silver ultrathin sections, mounted on copper grids, were stained with uranyl acetate–lead nitrate and examined with a Zeiss EM10 electron microscope.

Plasma membrane integrity. Plasma membrane integrity was assessed by trypan blue exclusion testing on the monolayer or on cells spun down from the medium. Monolayers were washed twice with Ca,Mg–PBS (i.e., PBS containing 0.68 m*M* $CaCl_2$ and 0.49 m*M* $MgCl_2$), covered with 0.1% (w/v) trypan blue in PBS, and observed in an inverted microscope. Cells from media were suspended in the trypan blue solution and the percentage of positive cells was evaluated in a hemocytometer.

DNA distribution by flow cytometry. DNA staining was performed as described [8, 12]. Cells were harvested by trypsinization, washed with ice-cold PBS, and fixed in 70% ice-cold ethanol for at least 30 min. After centrifugation, cells were incubated at room temperature in the presence of DNase-free RNase (Type 1-A) and propidium iodide (PI) at final concentrations of 0.4 and 0.18 mg/ml PBS, respectively. Fluorescence was measured using a FACScan flow cytometer (Becton–Dickinson, Mountain View, CA) equipped with a 488-nm argon laser. Two filters were used to collect the red fluorescence due to PI staining the DNA, one transmitting at 585 nm with a bandwidth of 42 nm (FL2), the other transmitting above 620 nm (FL3). FL2 and FL3 were registered on a linear and on a log scale, respectively. Simultaneously, forward (FSC) and side light scatter were measured as well. At least 10^4 cells were analyzed for each sample, at a flow rate of about 200 cells/s. Debris were excluded from analysis by appropriately raising FSC and FL3 thresholds to values selected experimentally [13]. Data were recorded in a Hewlett Packard computer (HP 9000, Model 300), using CellFit software (Becton–Dickinson).

Tissue transglutaminase (tTG). For enzyme assays, monolayers were washed with PBS and cells detached with a rubber policeman, then sonicated for 30 s at 4°C in 50 m*M* Tris–HCl, pH 8.4, containing 1 m*M* EDTA. tTG activity was measured as incorporation of [^{3}H]-putrescine into N,N′-dimethylcasein by the method of Folk and Cole [14], with some modifications by Piacentini *et al.* [15]. Briefly, 100–200 μg cell protein was incubated in an oscillating bath at 37°C for 30 min in a reaction mixture containing 50 m*M* Tris–HCl, pH 8.4, 30 m*M* NaCl, 5 m*M* $CaCl_2$, 10 m*M* dithiotreitol, 0.2 m*M* cold putrescine, 2 μCi [^{3}H]putrescine, and 2.5 mg/ml dimethylcasein, in a final volume of 0.3 ml. An aliquot of the incubation mixture was then layered onto filter paper (Whatman; 3MM) and, after extensive washing with cold 5% trichloroacetic acid containing 0.2 *M* KCl, its radioactivity was counted. Activity was expressed as nanomoles of [^{3}H]-putrescine incorporated per milligram of protein/hour.

For immunocytochemistry, cells grown on chamber slides were stained with the biotin–avidin technique as detailed elsewhere [16]. Affinity-purified monospecific rabbit immunoglobulins raised against tTG purified from human erythrocytes were used as first antibody, and biotinylated goat anti-rabbit immunoglobulins as second antibody. Slides were incubated overnight in a humidified chamber at 4°C, then treated with an avidin–horseradish peroxidase complex; the reaction was developed using aminoethylcarbazole and H_2O_2 as chromogenic substrate. Methanol–H_2O_2 was used to block endogenous peroxidase. Nuclei were counterstained with Mayer's hemalum.

DNA electrophoresis. DNA was extracted and electrophoresed by standard procedures as described by Kaufmann [17], with minor modifications. Monolayers were washed with PBS and cells were harvested mechanically and incubated ($2–4 \times 10^6$ cells/2 ml) overnight at 48°C in a lysis buffer that contained 500 m*M* Tris–HCl, pH 9, 2 m*M* EDTA, 10 m*M* NaCl, 200 μg/ml proteinase K, and 1% (w/v) sodium dodecyl sulfate. Cell lysates were sequentially extracted with phenol (pH 8), phenol:chloroform:isoamyl alcohol (25:24:1), and chloroform:isoamyl alcohol (24:1). DNA was precipitated overnight with 0.1 volume 3 *M* Na acetate and 2.5 volumes absolute ethanol at −20°C and sedimented at 5000*g* for 30 min. The pellet was rinsed with 70% ethanol and air dried. DNA was then dissolved in 10 m*M* Tris–HCl buffer, pH 8.0, containing 1 m*M* EDTA, and treated with DNase-free RNase (200 μg/ml) for 2 h at 37°C. DNA concentration and purity were checked spectrophotometrically from the absorbance at 260 and 280 nm. Approximately 10 μg DNA per lane was loaded onto 1.8% agarose gel containing 0.5 μg/ml ethidium bromide and 1 m*M* EDTA in 40 m*M* Tris–acetate buffer, pH 8.0, and run for 1 h at 50 V, then for 2 h at 75 V. Gels were photographed under UV illumination.

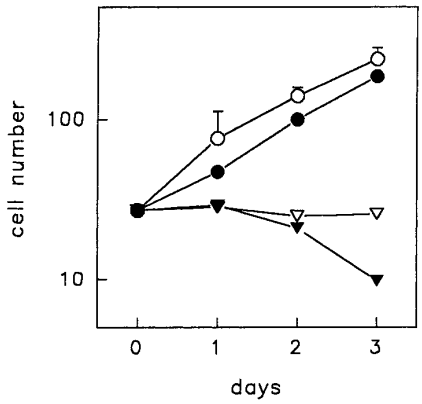

FIG. 1. Effects of VP-16 on growth of L929 cells. Controls (○) and cultures continuously exposed to 0.1 (●), 1 (▽), and 10 μM (▼) VP-16. Cellularity in monolayers evaluated by Coulter counting of cells detached by trypsinization and expressed as 10^{-4} cells/cm^2. Each point is the mean of triplicate determinations on six separate experiments; vertical bars represent standard deviations (not shown if their size did not exceed that of symbols).

DNA synthesis and loss. Exponential L929 cell cultures were grown in the presence of [^{3}H]thymidine (0.1 μCi/ml) over three to four population doublings to label DNA homogeneously. Then cells were washed twice with PBS, seeded at the usual density, chased for 24 h in cold medium, further washed twice in DMEM, and shifted to VP-16-containing medium. At the times indicated monolayers were carefully washed thrice with PBS, cells were detached with a rubber policeman and homogenized in Ca,Mg–PBS by sonication, and aliquots were transferred to scintillation vials, solubilized overnight at 50°C with Hyamine hydroxide, mixed with Ultima Gold as scintillation liquid, and counted for radioactivity in a LS 1801 spectrometer (Beckman, U.S.A.). Fractional rates of DNA synthesis (k_s) and loss (k_l), expressed as percentage per day, were calculated by linear regression from the log decay of specific (dpm/mg DNA) and total (dpm/dish) radioactivities, respectively [18]:

$$k_s = \ln(\text{specific radioactivity})\ \text{day}^{-1},$$

$$k_l = \ln(\text{total radioactivity})\ \text{day}^{-1}.$$

Chemicals. DMEM was purchased from Biochrom-Seromed (Berlin, Germany); DAPI from Boehringer (Mannheim, Germany); Hyamine hydroxide and Ultima Gold from Packard (Groningen, Holland); etoposide, RNase A, proteinase K, and agarose matrix gel from Sigma; LX112 from Polysciences, Inc. (U.S.A.); [^{3}H]thymidine (5 mCi/mmol) from Amersham (UK); and [^{3}H]putrescine (30 Ci/mmol) from DuPont NEN (Germany). Anti-tTG immunoglobulins were a kind gift from Professor Laszlo Fesus, Department of Biochemistry, Debrecen University Medical School, Debrecen, Hungary. All other reagents used were analytical chemistry or molecular biology grade.

RESULTS

Effect of VP-16 on Cell Growth

Unsynchronized, exponentially growing monolayers of L929 cells were continuously exposed to increasing concentrations of VP-16 over a 3-day period and the cell number was monitored (Fig. 1). While not significantly affected by 0.1 μM drug, growth was completely suppressed by 1 μM VP-16, and the cell number in the monolayer actually decreased during Days 2 and 3 with 10 μM VP-16. Even more severe effects were observed on higher (50–100 μM) drug exposures (not shown). Concurrently with these changes in the monolayer, there was a dose- and time-dependent increase in the number of cells floating in the media (see below). All subsequent experiments were performed with 1 or 10 μM VP-16.

Growth was also measured as total DNA (Fig. 2a) or total protein (not shown) per dish, with results similar to those reported above. However, the protein/DNA ratio progressively increased in treated cultures (Fig. 2b), due to the marked suppression of DNA synthesis (Fig. 2d) with no comparable decrease in protein accumulation [cf. 2].

Flow Cytometry

By DNA distribution, L929 monolayers exposed to 1 μM VP-16 showed a progressive depletion of the G0–G1 and S phases with a concurrent accumulation of G2–M cells (Fig. 3a). With 10 μM VP-16 the pattern was slightly different: S cell depletion was delayed and the whole population arrested by 24 h into a broader peak that also included the late S phase (Figs. 3b and 3c). In either case, the cell cycle blockade was maximal by 24 h and persisted unmodified thereafter. These findings are in agreement with previous observations made on the same [8] or different [19–21] types of cells.

After 24 h on VP-16 a subpopulation emerged that exhibited a DNA fluorescence $\leqslant$10% of the 2n value, manifesting in a region of the cytogram quite "distal" to the G0–G1 peak. Such A0 region [22, 23], corresponding to apoptotic cells, was first prominent in the medium and, after Day 2, clearly detectable in the monolayer as well (Fig. 4). Figure 5b shows the overall accumulation of apoptotic (A0) cells in treated cultures (monolayers plus media). These data clearly indicate that cell death by 1–10 μM VP-16 only occurred after growth arrest in (late S)–G2–M had established; the duration of the lag between the two processes remains undetermined, however, for both were asynchronous [7].

Light Microscopy

Cells exposed to VP-16 (Fig. 6) soon lost their typical spindle-shaped morphology and were all rounded off by 4–6 h, when most of them began to exhibit a pronounced surface blebbing (not shown). Treated cells gradually increased in size, consistent with both the unbalanced growth (Fig. 2) and the arrest in late cell cycle phases (Fig. 3). Chromatin condensed into discrete irregular clumps, often adjacent to the nuclear

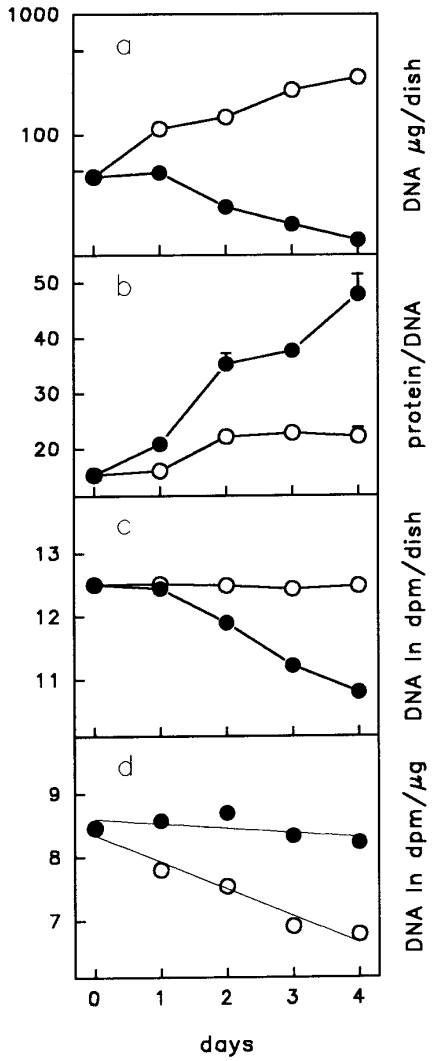

FIG. 2. Effects of VP-16 on protein/DNA ratio and on rates of DNA synthesis and loss in L929 cell monolayers. Cells homogeneously labeled with [^{3}H]thymidine, subcultured for the times indicated in the absence (○) or in the presence (●) of 10 μM VP-16, then harvested by trypsinization and assayed for protein and DNA content and for DNA radioactivity. (a) Total DNA per dish, (b) protein/DNA ratio, (c) log decay of total (dpm/dish) DNA radioactivity, and (d) log decay of specific (dpm/mg) DNA radioactivity (see Materials and Methods for details). Data illustrate one of three separate experiments, which provided similar results, each employing at least six separate dishes per point with triplicate assays. Vertical bars represent standard deviations (not indicated when their size did not exceed that of symbols).

membrane, while mitotic figures progressively disappeared. After 24 h of treatment small round eosinophilic bodies with a sharp smooth outline (Fig. 6C) and a variable content of DAPI-stained DNA (Figs. 7A and 7B) appeared in the monolayer. Quite sparse initially, these bodies progressively increased in number, up to 23% of monolayer cells by Day 3 on exposure to 10 μM VP-16 (Fig. 5a). Clearly, this apoptotic index in the monolayer is significantly lower than that measured by flow cytometry on monolayers and media combined (Fig. 5b). As shown below (see *Electron Microscopy*), a considerable number of apoptotic bodies could be sedimented by centrifugation from the media of cultures exposed to VP-16.

The eosinophilic bodies often appeared adhering to, or in the process of being engulfed by, viable cells; similar bodies were frequently observed in intracellular vacuoles (Fig. 6D). These observations suggest that in VP-16-treated cultures apoptotic bodies underwent homophagocytosis (phagocytosis by homotypic cells), as previously reported for apoptosing L cells exposed to excess thymidine [1, 2].

When directly tested on monolayers, virtually all cells (⩾98%) treated with VP-16 excluded trypan blue, comparable to control untreated cultures. By contrast, 30–40% of the cells in the medium were permeable to the dye. These data are consistent with those provided by propidium iodide exclusion test analyzed by flow cytometry [8].

Electron Microscopy

Spindle-shaped control L929 cells rounded up during the harvesting process (Fig. 8A). These cells showed microvilli protruding from the entire surface, well-preserved cytoplasmic organelles, smoothly outlined nuclei, and chromatin either finely dispersed or partly in the form of heterochromatin. After exposure to VP-16 (Fig. 8B), microvilli progressively disappeared, the plasma membrane protruded into numerous blebs, mostly containing free ribosomes, particularly evident by Day 1. Mitochondria exhibited an increasingly heterogeneous morphology, the endoplasmic reticulum showed some degree of microvacuolation, Golgian areas and autophagic vacuoles were quite prominent. The nuclear outline became irregular and developed multiple deep indentations that conferred a polylobated appearance to the nucleus. Chromatin condensed into clumps, most of which abutted the nuclear membrane. Consistent with light microscopic observations, we found no fragmentation of cells into multiple apoptotic bodies by electron microscopy. Rather, individual cells appeared to collapse into single dense bodies with a smooth continuous outline. In the cytoplasm of many VP-16-treated cells, though never of control cells, a striking feature was the presence of clear, roughly parallel clefts partly delimited by membranes and often containing some apparently free-floating membranes (Fig. 8B). While these clefts likely are artifacts generated in the course of the structural rearrangement that follows cell detachment from the substrate, they presumably reflected some peculiar structural changes in

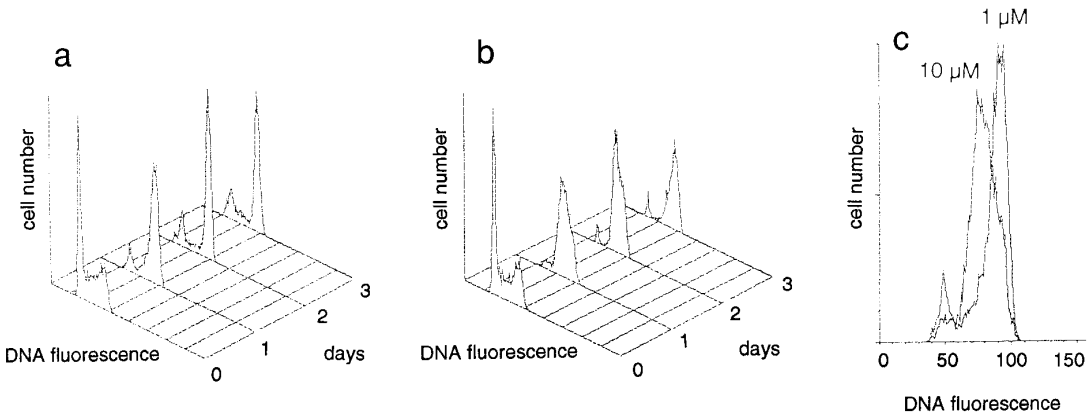

FIG. 3. Cell cycle distribution of L929 cells exposed to VP-16. Representative histograms of the DNA fluorescence (linear scale) analyzed by flow cytometry on monolayer cells detached by trypsinization. Only the portion of the cytograms corresponding to the conventional cell cycle phases is represented. Cultures exposed to 1 (a) or 10 (b) μM VP-16 for the times (days) indicated on the axis; (c) histograms at Day 1 superimposed to stress the difference between patterns. In controls, the distribution did not change appreciably from that at t_0.

the cytoplasm that were only observed in L929 cells exposed to VP-16. Their precise nature was not established in the present work, however.

Typical apoptotic bodies were observed among cells recovered from the monolayers, though their number

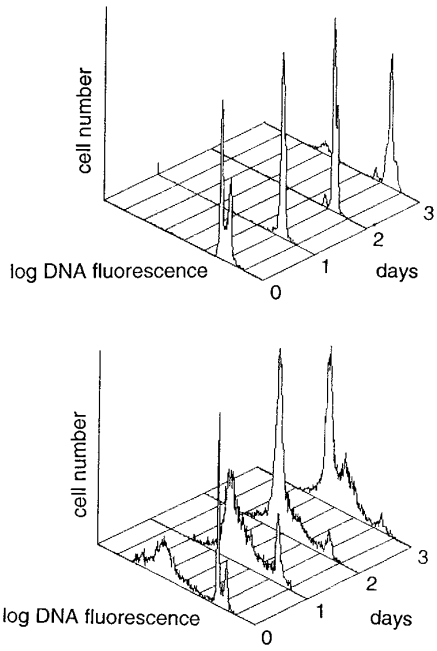

FIG. 4. DNA fluorescence distribution of cells recovered from the medium. Cells from the monolayer (top) or from the medium (bottom) of cultures exposed to 10 μM VP-16 for the times indicated. Cytograms show the full distribution of DNA fluorescence on a log scale. The A0 region was identified empirically and debris excluded choosing appropriate thresholds for FSC and FL3 channels as detailed elsewhere ([8], particularly Fig. 5).

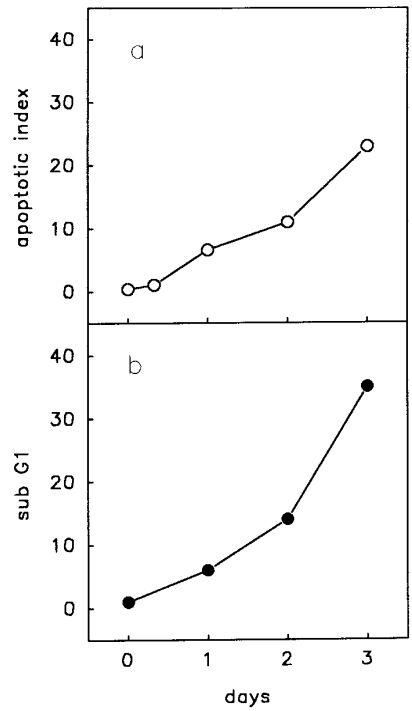

FIG. 5. Frequency of apoptotic cells in L929 cell cultures exposed to 10 μM VP-16. (a) Apoptotic index as determined by light microscopic counting on monolayers grown on chamber slides and stained with hematoxylin and eosin; in controls (not shown) the apoptotic index was negligibly low and did not appreciably change with time in culture. (b) Total number of apoptotic bodies in L929 cell cultures (monolayers plus media) as estimated by flow cytometry on the basis of the subdiploid DNA fluorescence [cf. 12]. Each point is the mean of six experiments (standard deviation bars not shown because their size did not exceed that of symbols).

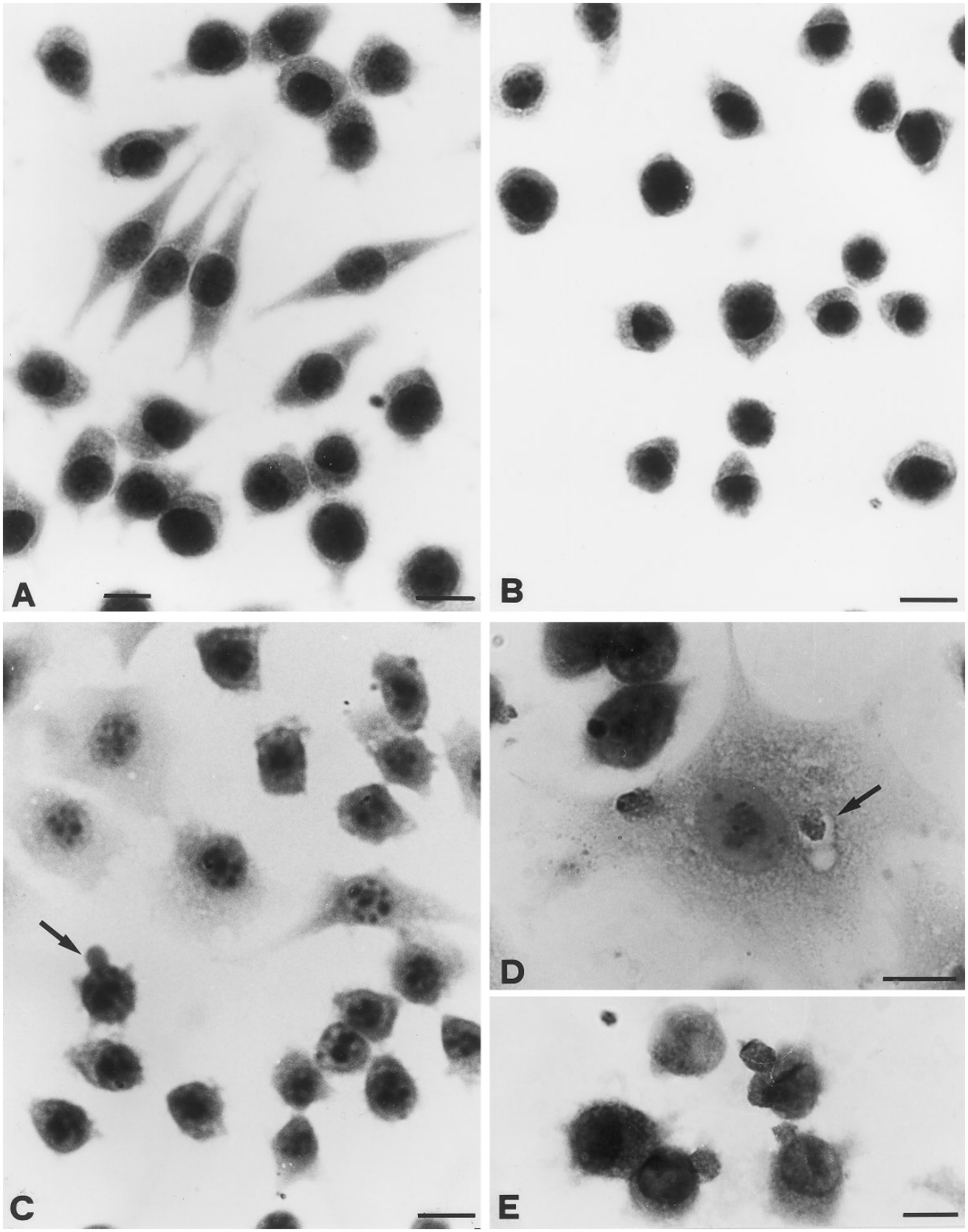

FIG. 6. Light microscopy of L929 cells exposed to 10 μM VP-16. Cells grown on chamber slides and stained with hematoxylin and eosin. Untreated cultures (A), typical morphology of L929 cells. Cultures treated with 10 μM VP-16: (B) 8 h, all cells have rounded off; (C) 24 h, chromatin shows condensation and apoptotic bodies (arrow) begin to appear; (D and E) 48 h, numerous apoptotic bodies are present, some adhering to flat cells, a few contained within intracellular vacuoles (arrow). Bars, 20 μm.

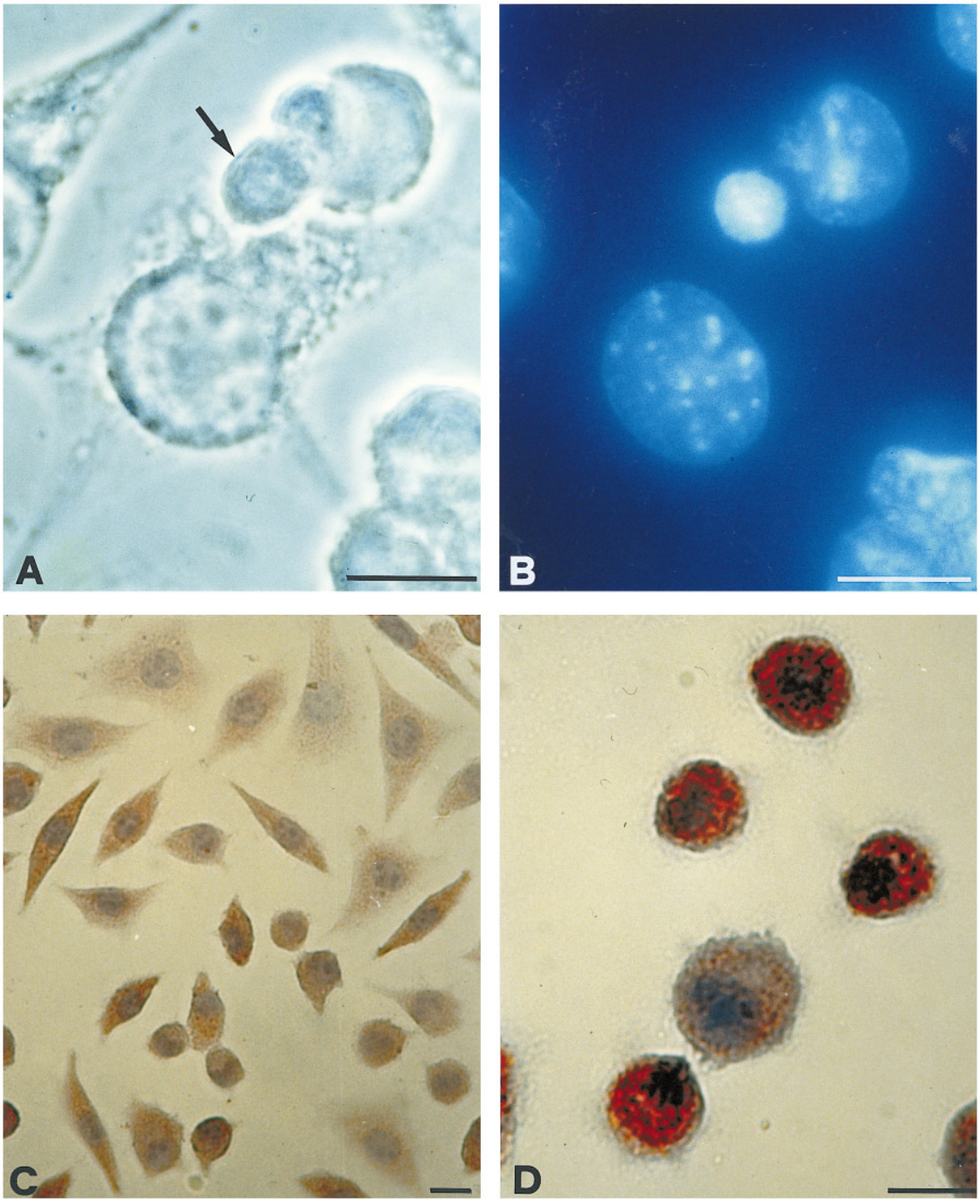

FIG. 7. Cytochemistry of L929 cells exposed to 10 μM VP-16. (A and B) Monolayers treated for 48 h and stained with DAPI. Phase-contrast (A) and fluorescence (B) microscopy of the same field: some cells show chromatin clumping, and only one (arrow) of two contiguous apoptotic bodies contains condensed DNA. (C and D) Immunocytochemical staining for tTG: (C) controls and (D) cells treated for 16 h. The apoptotic bodies seen since 24 h were all strongly positive (not shown). With preimmune serum (rabbit IgG) as primary antibody there was no detectable cell staining at any time of treatment (not shown). Bars, 20 μm.

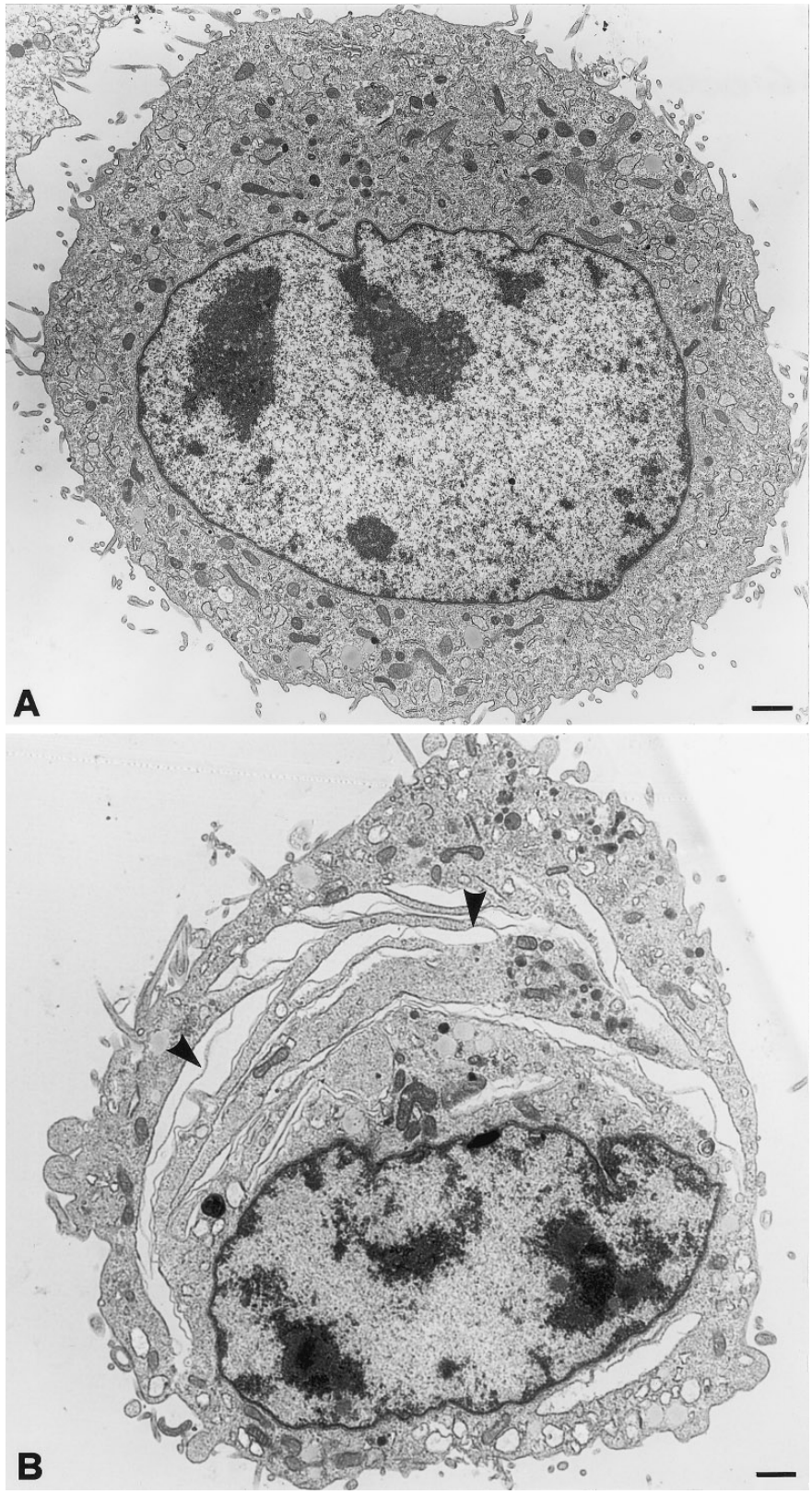

FIG. 8. Transmission electron microscopy of L929 cells harvested from the monolayer. (A) Cell in a control culture and (B) early apoptotic cell cultured for 48 h in the presence of 10 μM VP-16. (A) Numerous microvilli project from the cell surface; chromatin is mostly dispersed. (B) Microvilli have largely disappeared; several clefts (arrowheads) partly delimited by membranes are evident in the cytoplasm; chromatin is condensed and partially marginated. Original magnification 6000×. Bars, 1 μm.

became substantial only on Days 2 and 3. Morphologically, they did not differ from the best preserved apoptotic bodies recovered from the medium and their description is thus given together (Figs. 9A and 9B). Smaller in size than monolayer cells (as exemplified in Fig. 8B), these bodies showed markedly shrunken cytoplasm and nucleus. Chromatin was heavily condensed up to frank pyknosis, nuclei had a variable morphology, and the nuclear envelope often showed obvious discontinuities (Fig. 9B, arrowheads). Clusters of highly electron-dense 30-nm particles were often seen both in the nucleus or free in the cytoplasm (Fig. 9B, arrow); noteworthily, similar structures have also been observed in HL-60 cells undergoing apoptosis by actinomycin D [24; also, C. Tacchetti *et al.* submitted]. Cytoplasmic organelles, in part well-preserved but also showing various degrees of deterioration, were often located to one side of the cell (Figs. 9A and 9B). Other apoptotic bodies (Figs. 9A–9C) exhibited pronounced signs of "secondary necrosis" [25]. Chromatin was lost from the nucleus, suggesting extensive chromatinolysis, cytoplasm showed an extensive microvacuolation with clearly damaged organelles, and discontinuities in the plasma membrane became evident. Thus the apoptotic bodies released to the medium appeared to evolve into heavily degraded cell ghosts and fragments that could be sedimented from the media (Fig. 9D).

Biochemical Markers of Apoptosis

The death process induced by VP-16 was further characterized by evaluating tTG in the cell monolayer. tTG activity, assayed as incorporation of [^{3}H]-putrescine into casein, by 6 h was increased sixfold in VP-16-treated cultures and remained elevated at least until 24 h (Fig. 10). An increased tTG protein content in VP-16-treated cells was suggested by the immunocytochemical patterns obtained with a polyclonal anti-human tTG antibody that cross-reacts with mouse tTG. While only part of the control cells were slightly stained (Fig. 7C), most treated cells were markedly positive (Fig. 7D) and the apoptotic bodies were heavily stained (not shown).

By standard agarose gel electrophoresis (Fig. 11), no evidence of internucleosomal DNA fragmentation could be detected in the course of the death process elicited by VP-16, within 72 h, similar to previous observations on L cells undergoing apoptosis by excess thymidine [2].

Cell Turnover

To estimate cell death rates, we labeled DNA in L929 cells homogeneously with [^{3}H]thymidine prior to exposing cultures to VP-16; DNA radioactivity was then assayed daily in the monolayer. The fractional rate of total DNA radioactivity loss measured over the Day 1–4 interval (Fig. 2c) increased from 0.2% day^{-1} in controls to 21% day^{-1} in cultures exposed to 1 μM VP-16 and to 57% day^{-1} in cultures on 10 μM VP-16 (Table 1). Concurrently, as estimated from the decay of specific DNA radioactivity in the same monolayers (Fig. 2d), DNA synthesis was suppressed in VP-16-treated cultures, from an average fractional rate of 43% day^{-1} in controls to 26% day^{-1} on 1 μM VP-16 and to 12% day^{-1} on 10 μM VP-16.

The assumption that total DNA radioactivity decay in the monolayer basically measured DNA loss and thus cell death was justified considering that: (i) dead cells either spontaneously detached from the monolayer (as shown above) or, being loosely attached, were mostly removed by extensive washing; (ii) having a very low DNA content (as shown above), the residual apoptotic bodies in the monolayer would contribute only negligible radioactivity to the total DNA pool measured; and (iii) as already observed in thymidine-treated L cell cultures [26; also, J. S. Amenta *et al.*, manuscript in preparation], little of the label released to the medium was reincorporated into cell DNA during the experimental period. With regard to the latter point, most of the label in an acid-soluble form in the medium was probably associated with small DNA fragments rather than free thymidine; in addition, little radioactivity was available for recycling from the phagocytosed apoptotic bodies. In any event, since an increased label recycling would only cause DNA loss to be underestimated, the changes in the rates obtained from VP-16-treated cultures can be regarded as minimum estimates of the actual changes in the rates of cell death and cell proliferation.

DISCUSSION

The Cell Death Process

The present observations show that continuous exposure to 1–10 μM VP-16 caused unsynchronized proliferating L929 cells to gradually arrest in the cycle and then to progress to apoptosis. By flow cytometry, cells on 1 μM VP-16 accumulated in G2–M, while on 10 μM drug they formed a broader peak that also included the late S phase. Since microscopically there was no evidence for an increase of mitotic cells, the arrest was likely located in the G2 and late S phases only. The blockade was maximal at 24 h, after which time an asynchronous process of cell death progressively developed in the monolayer, exhibiting light and electron microscopical features characteristic of apoptosis: pronounced cell shrinkage into round bodies, chromatin condensation up to frank pyknosis, compaction of the cytoplasm with relatively well preserved organelles,

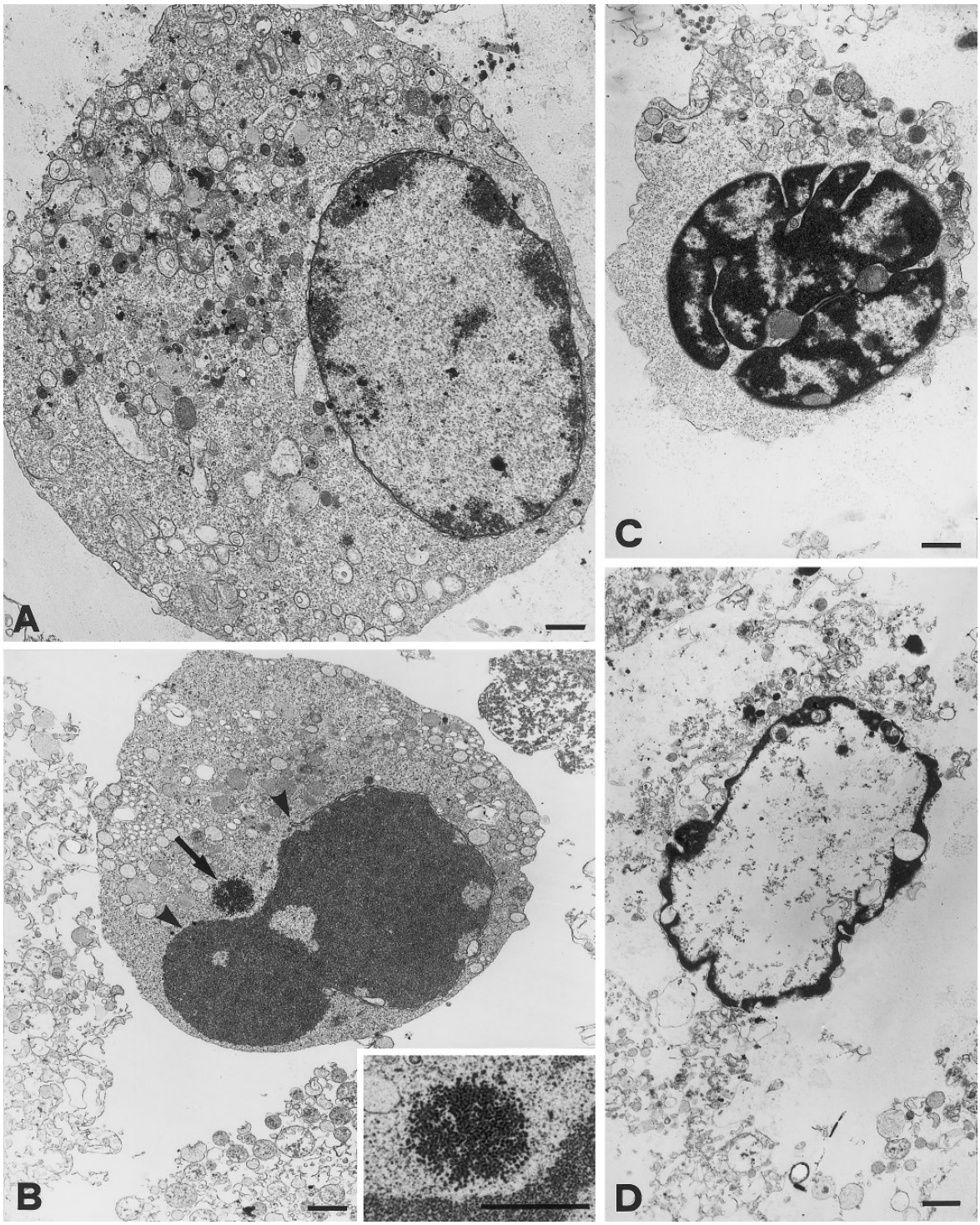

FIG. 9. Transmission electron microscopy of apoptotic bodies or cell remnants sedimented from the medium of L929 cell cultures exposed to 10 μM VP-16 for 72 h. (A) Smooth nuclear outline with some dilations of the nuclear membrane, chromatin largely condensed in masses abutting the nuclear membrane, compacted cytoplasm with recognizable organelles, smooth cell surface. (B) Heavily condensed chromatin in an apparently bilobated nucleus, with wide discontinuities of the nuclear envelope (arrowheads) and an extranuclear cluster of 30-nm electron-dense particles (arrow, and see inset). (C) Highly convoluted nuclear membrane, heavy chromatin condensation, cytoplasmic organelles clustered in the upper right part of the body, plasma membrane with large discontinuities. (D) Cell remnant mostly represented by an extensively degraded nucleus with a peripheral rim of condensed chromatin. Magnification 6000× (inset 17,000×). Bars, 1 μm.

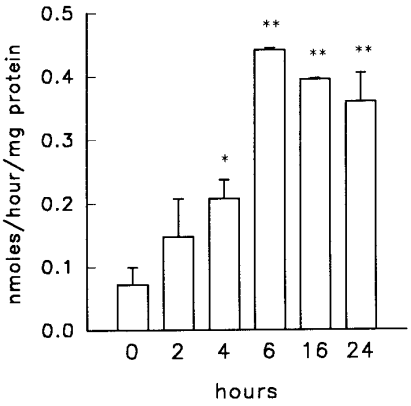

FIG. 10. Transglutaminase activity in L929 cell monolayers exposed to 10 μM VP-16. Data are means of three experiments, vertical bars indicate SD. Activity was assayed, in triplicate, as incorporation of [^{3}H]putrescine into N,N′-dimethylcasein (see Materials and Methods). Significance of differences by analysis of variance: *, $P < 0.05$; **, $P < 0.01$.

blebbing, loss of microvilli, and eventual smoothing of the cell surface.

A significant step was the release of the dead cells from the monolayer to the medium. While virtually all cells in the monolayer, including apoptotic bodies, excluded trypan blue (or propidium iodide [8]), a substantial proportion (30–40%) of the bodies in the medium did not. This suggested that permeabilization of the plasma membrane to trypan blue developed after apoptotic bodies had formed. Such permeabilization should probably be regarded as one aspect of a process of secondary necrosis/cell lysis that occurred in the apoptotic

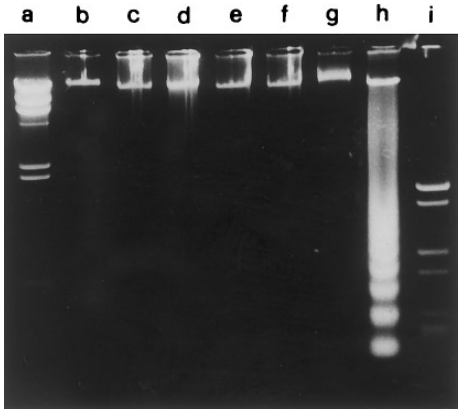

FIG. 11. Agarose gel electrophoresis of DNA from VP-16-treated L929 cells. Size markers ranging from 23 to 0.6 kb (lane a) and from 1.7 to 0.2 kb (lane i). L929 cells: controls (lane b) and cells exposed to 10 μM VP-16 for 6, 24, 48, and 72 h (lanes c, d, e, and f, respectively). HL-60 cells treated with 100 μM VP-16 for 0 and 6 h (lanes g and h, respectively) as positive control.

TABLE 1

Growth Kinetic Parameters in L929 Cell Monolayers Exposed to VP-16

	Day	k_s	k_d	$k_s - k_d$	k_a
Controls	0–4	43	0.2	43	47
1 μM VP-16	1–4	26	21	5	0
10 μM VP-16	1–4	12	57	−45	−43

Note. Fractional rate constants, expressed as %day^{-1}. Rates of cell production and of cell loss (k_s and k_d) were calculated (see Materials and Methods) from the decay of specific and total DNA radioactivities, respectively (the experimental data shown in Figs. 2c and 2d). k_a = ln(cell number) day^{-1} is the observed accumulation rate, calculated from total DNA per dish (data shown in Fig. 2a). $k_s - k_d$ corresponds to the accumulation rate calculated by difference.

bodies, as observed by electron microscopy (see below). Altogether, flow-cytometric and microscopical data indicate that in L929 cultures growth arrest by 1 or 10 μM VP-16 was followed by an asynchronous process of cell death, by which cells initially shrank into trypan blue-excluding bodies, then became detached from the substrate and were released into the medium, and eventually became permeable to the dye and lysed.

Persistence of dye exclusion by the plasma membrane not only is a hallmark of cell death by apoptosis [25], however often neglected, but likely also has a precise mechanistic significance. Maintenance of appropriate gradients for ions such as H^+, K^+, Na^+, and Ca^{2+} is critical for L929 cells exposed to VP-16 to die by apoptosis, since interfering with their control caused cells to die earlier and by the necrotic mode [8]. Moreover, important shifts in the intracellular concentration of monovalent cations, and particularly extrusion of K^+, may be instrumental in the final collapse of cells into apoptotic bodies [8].

The observation that tTG activity and immunocytochemical staining increased, in L929 cells exposed to VP-16, is compatible with an involvement of tTG in the cell death process [3, 27–29]. Evidence for an actual cross-linking of cell proteins associated with the formation of apoptotic bodies has been obtained (F. Duranti *et al.*, unpublished observations). tTG activity is known to increase when cell proliferation declines [28, 30–32], yet the kinetics of the present change suggests that some regulation other than the observed growth arrest was involved as well. However, the molecular basis for the enhanced tTG activity, whether by activation [28, 33] or by increased enzyme content [31], was not assessed in the present work, though the immunocytochemical patterns are suggestive for an increased tTG protein content in VP-16-treated cells. The precise relation of tTG changes to protein cross-linking and the role played by intracellular Ca^{2+} shifts [8] in modulat-

ing the activity of a Ca^{2+}-dependent enzyme such as tTG in cells bound to apoptose remain to be elucidated.

No internucleosomal DNA fragmentation could be detected by agarose gel electrophoresis at any time during the 3-day treatment of L929 cells with VP-16, a result not different from that previously reported on a similar apoptosis model, i.e., L cells exposed to excess thymidine [2]. This is no longer an exceptional finding in studies on apoptosis [e.g., 4, 6, 34–36], irrespective of the initiating role that DNA cleavage into high-molecular-weight fragments might play in particular situations [4, 37]. On the other hand, cleavage of DNA into high-molecular-weight fragments [cf. 38] could be detected in VP-16-treated L929 cells (F. Duranti *et al.*, unpublished observations). Moreover, in L929 cell cultures treated with either thymidine [8] or VP-16, such as in the current work, the apoptotic cells show a greatly reduced DNA fluorescence, down to $\leqslant$10% of the 2*n* levels ("distal" subdiploid peak in cytograms), suggesting that extensive degradation of DNA had occurred. This apparent inconsistency is likely accounted for by the asynchrony of the cell death process as well as by the rapidity by which DNA is extensively degraded to subnucleosomal fragments in apoptosing cells [39; also, J. S. Amenta *et al.*, manuscript in preparation]. Noteworthily, however, a clearcut DNA "ladder" has indeed been observed for L929 cells, not only in other models of apoptosis [40–42], but also after 4 days on 10 μM VP-16 [43]. The reason for the discrepancy between the latter and the present findings could reside in the particular L929 cells used or in some detail of the cell lysis and DNA extraction procedure. Of interest, we can generate a DNA ladder as a transient pattern by incubation of untreated L929 cells in a Triton X-100–EDTA–Tris buffer at a moderately acidic pH (unpublished observations). However, a thorough discussion of this issue goes beyond the scope of the present work and will form the object of a separate article (J. S. Amenta *et al.*, manuscript in preparation).

VP-16 is widely used as anticancer agent and has recently become a popular apoptogenic agent [e.g. 8, 20, 21, 38, 43–47]. The mechanism of its toxic action on cells is not completely understood [reviewed in 48–50]. The drug interacts with topo II, stabilizing the so-called cleavable complex, an intermediate in the catalytic cycle in which the enzyme is covalently bound to DNA. Stabilization of the cleavable complexes, inhibition of DNA replication, DNA damage, cell cycle arrest, and blockade at a topo II-sensitive G2 checkpoint [51] are among the effects of VP-16 that could mediate its cytotoxicity. In general, cells of different types may exhibit a wide spectrum of responses to VP-16 with regard to susceptibility (effective drug concentrations or exposure times), kinetics of the cytotoxic effect, or even mode of cell death (apoptosis versus necrosis). At one extreme, resistance to VP-16 has been related to low expression or mutations of topo II [e.g., 52] as well as to GRP78 overexpression [53]. At the other, cells such as HL-60 [20, 54–55, and unpublished data] can be killed by VP-16 in a few hours only. In the present work, a few hours were sufficient for VP-16 to elicit drastic changes in L929 cell shape, although apoptotic death became detectable only later. Moreover, while the extent of cell cycle blockade afforded by 1 or 10 μM VP-16 was comparable, the latter drug concentration caused cell death rates three times higher than the former, suggesting that lethality involved factor(s) other than mere arrest in the cycle.

Quantification of Cell Death

Rates of cell loss in the present model system were assessed by a conventional, quite simple procedure: the log decay of total DNA radioactivity from monolayers homogeneously prelabeled with [^{3}H]thymidine. In addition to the validations ordinarily required in such measurements, two assumptions were needed in the present work: (i) that DNA radioactivity decay in the monolayer was a reliable measure of cell loss and (ii) that cell death was determined only by apoptosis. The first assumption has already been discussed under Results, the second one is supported by any parameters investigated in the present as well as in other work [8, unpublished data]. We could thus estimate that in L929 monolayers apoptosis accounted for increases in the rate of cell loss from 0.24% day^{-1} in exponentially growing controls to an average 21 and 57% day^{-1} in cultures exposed to 1 and 10 μM VP-16, respectively (Table 1).

Comparing these rates with the number of apoptotic bodies counted in monolayers by light microscopy or the number of sub-G1 bodies measured by flow cytometry on monolayers plus media clearly shows that the latter "static" parameters largely underestimated the extent of the apoptotic process. In fact, these counts only measured the accumulation of apoptotic bodies in monolayer or in whole cultures, not the rate of the death process. This limitation holds even assuming, as the observations suggest, that each cell collapsed into a single apoptotic body, though fragmentation of cells into multiple bodies could not be ruled out completely. Most important in the present work is that the apoptotic bodies loosened their anchorage to the plastic substrate to float free in the culture medium. After an undetermined length of time their fate was then twofold: either (i) they underwent "secondary necrosis" that eventually led to extensively degraded ghosts and debris or (ii) they were subject to phagocytosis by homotypic cells (homophagy); that is, engulfment and degradation by still viable cells in the monolayer. From the

present data, it is not clear whether, or to what extent, the two processes were mutually exclusive. Examining monolayers grown on glass chamber slides, the bodies seen adhering to viable cells generally looked well-preserved and excluded trypan blue. This might suggest that, while recently formed bodies bore adequate molecular signals for their recognition and uptake by viable cells, these signals might have been compromised by secondary necrosis. Consistent with these post-apoptotic changes in the dye-excluding function of the plasma membrane, electron microscopy clearly indicated that cell envelopes were extensively damaged. On the other hand, still-viable cells in VP-16-treated monolayers contained many prominent structures that, though looking like autophagic vacuoles, could rather represent cellular debris internalized from the medium. Although further work is needed to assess this point, it is clear that in tissue cultures apoptotic bodies disappear by mechanisms similar to those that operate in tissues *in vivo*, i.e., lysis or phagocytosis. Therefore, when cell death is both asynchronous and relatively rare, such as in the present model system or in tissues, counts of the apoptotic bodies [e.g., 5, 8] only provide "snapshots" [56] of apoptotic cell death and no information about its rate.

Parts of this work have been presented in a preliminary form. We thank Professor Dario Cantino (Turin) for the use of the electron microscope and Professor Laszlo Fesus (Debrecen) for the anti-tTG antibodies. This study was supported by grants from the Associazione Italiana per la Ricerca sul Cancro (AIRC), Milan; the Consiglio Nazionale delle Ricerche (CNR, Special Projects ACRO and Aging), Rome; and the Ministero per l'Università e la Ricerca Scientifica e Tecnologica, Rome. Fellowships from AIRC (L.V.d.C., F.D.) and from the Fondazione Gigi Ghirotti, Turin, and then from CNR, Special Project Aging (Gi. Ba.), are acknowledged.

REFERENCES

1. Amenta, J. S., and Baccino, F. M. (1989) *Cell Biol. Rev.* **21,** 404–422.
2. Amenta, J. S., Sargus, M. J., Baccino, F. M., Sacchi, C., and Bonelli, G. (1993) *In Vitro Cell Dev. Biol.* **29A,** 855–861.
3. Fukuda, K., Kojiro, M., and Chiu, J. F. (1993) *Hepatology* **18,** 945–953.
4. Oberhammer, F., Wilson, J. W., Dive, C., Morris, I. D., Hickman, J. A., Wakeling, A. E., Walker, P. R., and Sikorska, M. (1993) *EMBO J.* **12,** 3679–3684.
5. Bayly, A. C., Roberts, R. A., and Dive, C. (1994) *J. Cell Biol.* **125,** 197–203.
6. Ormerod, M. G., O'Neill, C. F., Robertson, D., and Harrap, K. R. (1994) *Exp. Cell Res.* **211,** 231–237.
7. Sherwood, S. W., and Schimke, R. T. (1994) *in* Apoptosis (Mihich, E., and Schimke, R. T., Eds.), pp. 223–236, Plenum, New York.
8. Barbiero, G., Duranti, F., Bonelli, G., Amenta, J. S., and Baccino, F. M. (1995) *Exp. Cell Res.* **217,** 410–418.
9. Desjardins, L. M., and MacManus, J. P. (1995) *Exp. Cell Res.* **216,** 380–387.
10. Lowry, O. H., Rosebrough, N. J., Farr, A. L., and Randall, A. J. (1951) *J. Biol. Chem.* **193,** 265–275.
11. Boer, G. J. (1975) *Anal. Biochem.* **65,** 225–231.
12. Barbiero, G., Munaron, L., Antoniotti, S., Baccino, F. M., Bonelli, G., and Lovisolo D. (1995) *Cell Calcium* **18,** 542–556.
13. Bianciotto, V., Barbiero, G., and Bonfante, P. (1995) *Protoplasma* **188,** 161–169.
14. Folk, J. E., and Cole, P. W. (1966) *Biochim. Biophys. Acta* **122,** 244–252.
15. Piacentini, M., Sartori, C., Bargagli, A. M., and Argento-Ceru, M. P. (1986) *Biochem. J.* **234,** 435–440.
16. Piacentini, M., Fesus, L., Farrace, M. G., Ghibelli, L., Piredda, L., and Melino, G. (1991) *Eur. J. Cell Biol.* **54,** 246–254.
17. Kaufmann, S. H. (1989) *Cancer Res.* **49,** 5870–5878.
18. Amenta, J. S., and Sargus M. J. (1979) *Biochem. J.* **182,** 847–859.
19. Lock, R. B., and Ross, W. E. (1990) *Cancer Res.* **50,** 3761–3766.
20. Barry, M. A., Reynolds, J. E., and Eastman A. (1993) *Cancer Res.* **53,** 2349–2357.
21. Guano, F., Bernardi, R., Negri, C., Donzelli, M., Prosperi, E., Astaldi Ricotti, G., and Scovassi, I. (1994). *Cell Death Differ.* **1,** 101–107.
22. Nicoletti, I., Migliorati, G., Pagliacci, M. C., Grignani, F., and Riccardi, C. (1991) *J. Immunol. Methods* **139,** 271–279.
23. Telford, W. G., King, L. E., and Fraker, P. J. (1991) *Cell. Prolif.* **24,** 447–459.
24. Tacchetti, C., Fusaroli, P. F., Tenca, C., Zarcone, D., and Grossi, C. E. (1995) *Fund. Clin. Immunol.* **3,** 79.
25. Wyllie, A. H., Kerr, J. F. R., and Currie, A. R. (1980) *Int. Rev. Cytol.* **68,** 251–306.
26. Amenta, J. S., Mehta, J., and Baccino F. M. (1988) *in* Chemical Carcinogenesis: Model and Mechanisms (Feo, F., Pani, P., Columbano, A., and Garcea, R., Eds.), pp. 535–551, Plenum, New York.
27. Fesus, L., Davies, P. J. A., and Piacentini, M. (1991) *Eur. J. Cell Biol.* **56,** 170–177.
28. El Alaoui, S., Mian, S., Lawry, J., Quash, G., and Griffin, M. (1992) *FEBS Lett.* **311,** 174–178.
29. Melino, G., Annicchiarico-Petruzzelli, M., Piredda, L., Candi, E., Gentile, V., Davies, P. J. A., and Piacentini, M. (1994) *Mol. Cell. Biol.* **14,** 6584–6596.
30. Birckbichler, P. J., Orr, G. R., Patterson, M. K., Jr., Conway, E., and Carter, H. A. (1981) *Proc. Natl. Acad. Sci. USA* **78,** 5005–5008.
31. Nara, K., Aoyama, Y., Iwata, H., Hagiwara, H., and Hirose, S. (1992) *Biochem. Biophys. Res. Commun.* **187,** 14–17.
32. Korner, G., Deutsch, V. R., Vlodavsky, I., and Eldor, A. (1993) *FEBS Lett.* **330,** 41–45.
33. Dadabay, C. Y., and Pike, L. J. (1987) *Biochemistry* **26,** 6587–6591.
34. Bøe, R., Gjertsen, T., Vyntermyr, O. K., Houge, G., Lanotte, M., and Döskeland, S. O. (1991) *Exp. Cell Res.* **195,** 237–246.
35. Cohen, G. M., Sun, X. M., Snowden, R. T., Dinsdale, D., and Skilleter, D. N. (1992) *Biochem. J.* **286,** 331–334.
36. Schulze-Osthoff, K., Walczac, H., Droge, W., and Krammer, P. H. (1994) *J. Cell Biol.* **127,** 15–20.
37. Brown, D. G., Sun, X. M., and Cohen, G. M. (1993) *J. Biol. Chem.* **268,** 3037–3039.
38. Sun, X.-M., Snowden, R. T., Dinsdale, D., Ormerod, M. G., and Cohen, G. M. (1994) *Biochem. Pharmacol.* **47,** 187–195.

39. Sargus, M. J., Amenta, J. S., Duranti, F., Barbiero, G., Baccino, F. M., and Bonelli, G. (1995) *J. Cell. Biochem. Suppl.* **19B,** 298.
40. Kyprianou, N., Alexander, R. B., and Isaacs, J. T. (1991) *J. Natl. Cancer Inst.* **83,** 346–350.
41. Facchini, L. M., Chen, S., and Penn, J. Z. (1994) *Cell Growth Differ.* **5,** 637–646.
42. Wolvetang, E. J., Johnson, K. L., Krauer, K., Ralph, S. J., and Linnane, A. W. (1994) *FEBS Lett.* **339,** 40–44.
43. Mizumoto, K., Rothman, R. J., and Farber, J. L. (1994) *Mol. Pharmacol.* **46,** 890–895.
44. Catchpoole, D. R., and Stewart, B. W. (1993) *Cancer Res.* **53,** 4287–4296.
45. Kamesaki, S., Kamesaki, H., Jorgensen, T. J., Tanizawa, A., Pommier, Y., and Cossman, J. (1993) *Cancer Res.* **53,** 4251–4256.
46. Kaufmann, S. H., Desnoyer, S., Ottaviano, Y., Davidson, N. E., and Poirier, G. G. (1993) *Cancer Res.* **53,** 3976–3985.
47. Negri, C., Bernardi, R., Braghetti, A., Astaldi Ricotti, G. C. B., and Scovassi, A. I. (1993) *Carcinogenesis* **14,** 2559–2564.
48. Liu, L. (1989) *Annu. Rev. Biochem.* **58,** 351–375.
49. Gewirtz, D. A. (1991) *Biochem. Pharmacol.* **42,** 2253–2258.
50. Long, B. H. (1992) *Semin. Oncol.* **19,** 3–19.
51. Downes, C. S., Clarke, D. J., Mullinger, A. M., Giménez-Ablàn, J. F., Creighton, A. M., and Johnson, R. T. (1994) *Nature* **372,** 467–470.
52. Ritke, M. K., and Yalowich, J. C. (1993) *Biochem. Pharmacol.* **46,** 2007–2020.
53. Chatterjee, S., Cheng, M. F., Berger, R. B., Berger, S. J., and Berger, N. A. (1995) *Cancer Res.* **55,** 868–873.
54. Ritke, M. K., Rusnak, J. M., Lazo, J. S., Allan, W. P., Dive, C., Heer, S., and Yalowich, J. C. (1994) *Mol. Pharmacol.* **46,** 605–611.
55. Barbiero, G., Duranti, F., Goglio, G., Verdun di Cantogno, L., Martinis, O., Sacchi, C., Autelli, R., Sargus, M. J., Amenta, J. S., Baccino, F. M., and Bonelli, G. (1995) *Fund. Clin. Immunol.* **3,** 88–89.
56. Evan, G. I. (1994) *Trends Cell Biol.* **4,** 191–192.

Received February 12, 1996
Revised version received July 16, 1996